Showcasing research from the group of Prof. Woojin Jeon at Kyung Hee University, Republic of Korea

Modulation of the adsorption chemistry of a precursor in atomic layer deposition to enhance the growth per cycle of a TiO_2 thin film

Atomic layer deposition (ALD) has scarcely been utilized in industrial processes due to its low productivity, even though it possesses several advantages for improving device performance. In this study, we investigate the exact chemical reaction mechanism of the ALD to obtain a designated growth behaviour or property, theoretically and experimentally. This study provides significant implications for understanding the ALD reaction mechanism based on the DFT calculation.

As featured in:

See Woojin Jeon *et al.*, *Phys. Chem. Chem. Phys.*, 2021, **23**, 2568.

ROYAL SOCIETY OF CHEMISTRY

rsc.li/pccp

Registered charity number: 207890

PCCP

ROYAL SOCIETY OF CHEMISTRY

PAPER

View Article Online
View Journal | View Issue

Cite this: *Phys. Chem. Chem. Phys.*, 2021, **23**, 2568

Modulation of the adsorption chemistry of a precursor in atomic layer deposition to enhance the growth per cycle of a TiO_2 thin film

Yeonchoo Cho, †[a] Sang Hyeon Kim,†[b] Byung Seok Kim,†[c] Youngjin Kim[d] and Woojin Jeon *[c]

Received 7th August 2020,
Accepted 30th September 2020

DOI: 10.1039/d0cp04176a

rsc.li/pccp

Atomic layer deposition (ALD) has scarcely been utilized in large-scale manufacturing and industrial processes due to its low productivity, even though it possesses several advantages for improving the device performance. The major cause of its low productivity is the slow growth rate, which is determined by the amount of chemisorbed precursor. The slow growth rate of ALD has become even more critical due to the introduction of heteroleptic-based precursors for achieving a higher thermal stability. In this study, we investigated the theoretical and experimental chemisorption characteristics of the $Ti(CpMe_5)(OMe)_3$ precursor during the ALD of TiO_2. By density functional theory calculations, the relationship between the steric hindrance effect and the chemistry of a chemisorbed precursor was revealed. Based on the calculation result, a way for improving the growth per cycle by 50% was proposed and demonstrated, successfully.

Published on 01 October 2020. Downloaded by Kyunghee University on 3/24/2021 8:41:53 AM.

Introduction

Atomic layer deposition (ALD) has been attracting a lot of attention as the most promising thin film deposition technique owing to its superior characteristics, such as precisely controllable film thickness and composition, excellent uniformity and step coverage, and good adhesion.[1–6] Moreover, ALD has been employed in the deposition of various kinds of thin film materials, such as conventional metals[7–9] and metal oxides,[10–14] and emerging materials such as perovskites[15–19] and 2-dimensional materials.[20–25] Hence, ALD is useful not only in electronic device applications,[26–28] but also in passivation layer coating[29,30] and functional thin film coating.[31] However, the applicability of ALD is hindered in the industry because of its low growth rate during the fabrication process. This implies that the application of ALD can be dramatically improved by solving the low growth rate problem.

The growth rate of ALD is generally calculated by the deposited film thickness per cycle (growth per cycle (GPC)). GPC is affected by several process parameters, among which the amount of chemisorbed precursor (p_{chem}) is the most significant.[32,33] The p_{chem} value strongly depends on the surface chemistry. The chemistry of surface termination characterizes the density of the active site, where the precursor can be adsorbed chemically; further, the geometry of the precursor ligand limits the maximum density of p_{chem}, which is a result of steric hindrance. Generally, the number of activated sites on the substrate can be increased by introducing a surfactant. Several surfactants (generally based on carbon compounds) have been introduced for performing surface treatment to enhance the chemisorption of a precursor that increases the GPC successfully. However, the residual compound from the surfactant causes contamination, resulting in severe degradation of the electrical properties.[34] The maximum density of p_{chem}, which is governed by steric hindrance, limits the enhancement of p_{chem} upon increasing the adsorption site number when the surfactant is incorporated. Moreover, bigger ligands have been introduced recently in numerous metal–organic precursors for ALD,[35] thereby enhancing the influence of steric hindrance on the GPC. In this regard, the reduction in steric hindrance would effectively increase the GPC. The steric hindrance is influenced by the ligand geometry of the chemisorbed precursor; therefore, analysing the reaction that occurs between the surface termination group and the precursor is also important. However, only a few studies have elucidated the chemical reaction mechanism that occurs during the chemisorption of a precursor, thereby demonstrating a change in GPC due to steric hindrance.

[a] *Samsung Advanced Institute of Technology, Gyeonggi 16678, Korea*
[b] *Process Development Team, Semiconductor R&D Center, Samsung Electronics Co. Ltd., Gyeonggi 18448, Korea*
[c] *Department of Advanced Materials Engineering for Information and Electronics, Kyung Hee University, Gyeonggi 17104, Korea. E-mail: woojin.jeon@khu.ac.kr*
[d] *Soft Hybrid Materials Research Center, Korea Institute of Science and Technology, Seoul, 02792, Republic of Korea*

† These authors are equally contributed to this work.

This journal is © the Owner Societies 2021

Published on 01 October 2020. Downloaded by Kyunghee University on 3/24/2021 8:41:53 AM.

In this work, the GPC of TiO_2 ALD is enhanced by controlling the p_{chem} of Ti according to the surface termination chemistry. Furthermore, the mechanism involved in the GPC enhancement is revealed by investigating the chemical reaction between the surface termination and the precursor. The steric hindrance of p_{chem} has also been experimentally and theoretically estimated.

Experimental

We performed first-principles density-functional simulations and used Gaussian 16 for molecular simulations.[36] [Gaussian 16, Revision A.03] The B3LYP functional was used with a cc-pVTZ basis set and D3 dispersion correction.[37] For slab simulations, we used the Vienna Ab initio Simulation Package.[38] The Perdew–Burke–Ernzerhof functional was used with D3 dispersion correction.[37] The plane wave cut-off was 400 eV. The atomic structures were relaxed until the residual forces decreased to a value lesser than 0.02 eV A^{-1}. We prepared a rutile $TiO_2(110)$ slab as described by Zydor *et al.*[39] In the presence of chemisorbed water, the Ti precursor underwent chemisorption. Due to the steric hindrance between the precursor and the surface, the cyclopentadienyl (Cp) ligand and the methoxy ligands were more stable when they were parallel to the [−110] direction, compared to the [001] direction.

TiO_2 thin films were deposited in a shower-head type ALD reactor (iSAC research, iOV dX1) to obtain a single wafer of 6 in. diameter. $Ti(CpMe_5)(OMe)_3$ (synthesized by SK Trichem Co., Ltd, Korea) was employed as the Ti precursor, respectively. The canister of $Ti(CpMe_5)(OMe)_3$ was heated to 80 °C for obtaining an appropriate precursor vapor pressure. O_3 was the source of oxygen in TiO_2 ALD with a concentration of 200 g m^{-3}. For all the experiments, the thin film growth temperature (T_g) was 370 °C. All the TiO_2 thin films were deposited on a Ru (40 nm)/SiO_2 (100 nm)/Si substrate with the sequence consisting of $Ti(CpMe_5)(OMe)_3$ feeding, Ar purge, O_3 feeding, and Ar purge steps of 12, 15, 10, and 15 s, respectively. To measure the electrical properties, a metal–insulator–metal (MIM) capacitor was fabricated with a 30 nm thick RuO_2 top electrode (TE) using a metal shadow mask (with a 300 μm hole diameter). On the RuO_2 TE, an additional 50 nm thick Pt layer was deposited to improve the contact while probing. The RuO_2 TE layer was deposited by DC reactive sputtering using an Ru metal target under an Ar/O_2 atmosphere. After the TE deposition, post-metallization annealing (PMA) was performed at 400 °C for 30 m under 95% N_2 + 5% O_2 atmosphere inside a tube furnace. The film thickness was measured using spectroscopic ellipsometry (J. A. Woollam, ESM-300), X-ray fluorescence spectroscopy (XRF, Thermo Scientific ARL QUANT'X), and X-ray reflection spectroscopy (XRR, PANalytical X'Pert Pro). The chemical structure was analysed using X-ray photoemission spectroscopy (XPS, Sigma Probe). Glancing angle incident X-ray diffraction (GIXRD, PANalytical X'Pert Pro., incident angle of 0.5°) was used to examine the crystallographic structure of the deposited films. The electrical performance was studied by measuring the capacitance–voltage (C–V) and the current–voltage (I–V) using Hewlett Packard 4140B and 4194A, respectively. During the electrical tests, the TE was biased and the bottom electrode (BE) was grounded.

Results and discussion

The chemisorption behaviour of the Ti precursor was analysed, depending on the surface termination chemistry. The Ti precursor adsorption was a typical dissociative chemisorption. The OCH_3 ligand captured the surface hydrogen, which was released as a methanol molecule. The Ti precursor was strongly bound to the surface *via* the Ti–O bond. This interaction could be considered as a ligand exchange reaction from the frame of reference of the Ti precursor. The reaction was exothermic with a reaction energy of −1.25 eV. The $CpMe_5$ (Cp*) and OCH_3 ligands laid parallel to the [−110] direction. If they lie perpendicular to this direction, the stability decreases because of the steric hindrance between the Cp* ligand and the surface oxygen. Consequently, the TiO_2 ALD with the Ti precursor has a low GPC because the Ti precursor chemisorbs with the Cp* ligand and two OCH_3 ligands, thereby inducing severe steric hindrance. Hence, the GPC can be increased by altering the ligand chemistry of the chemisorbed Ti precursor. However, despite the induction of steric hindrance by the Cp* ligand, the Cp* ligand cannot be removed during the chemisorption because it improves the temperature stability of the precursor. Hence, we considered eliminating the OCH_3 ligand to reduce the steric hindrance.

To eliminate the OCH_3 ligand, H_2O was chosen for altering OCH_3 into OH, which exhibited a smaller size; this is because H_2O does not react with the Cp* ligand under moderate ALD process conditions.[40] Moreover, introducing H_2O in ALD is convenient due to the physisorption of H_2O, thereby rendering H_2O suitable for reducing the steric hindrance. The physisorbed water molecules have sufficient energy to react with the Ti precursors and reduce the steric hindrance in the Ti precursor pulse. Fig. 1 shows two ways in which the Ti precursor reacts with a water molecule. In the reactant state, one of the hydrogen atoms in the water molecule is hydrogen-bonded to the methoxy oxygen in the Ti precursor. This hydrogen atom can be transferred to the Ti precursor if a relatively small activation energy of 0.39 eV is applied. As a result, a methanol molecule is released and the Ti precursor becomes less bulky. There is also a possibility in which the hydrogen atom can be transferred to the Cp* ligand; however, this process requires more energy. In addition, the hydrogen in the initial reactant state prefers to interact with the oxygen in the methoxy ligand, rather than the carbon in the Cp* ligand. Thus, the release of methanol is preferred, as observed experimentally. However, the activation energy required for the Cp* detachment is not excessively large. At elevated temperatures, a chemical vapor deposition (CVD)-like non-self-limiting behaviour is expected. Note that the energies represented in Fig. 1 are internal energies. Although the internal energy of the product state is

Published on 01 October 2020. Downloaded by Kyunghee University on 3/24/2021 8:41:53 AM.

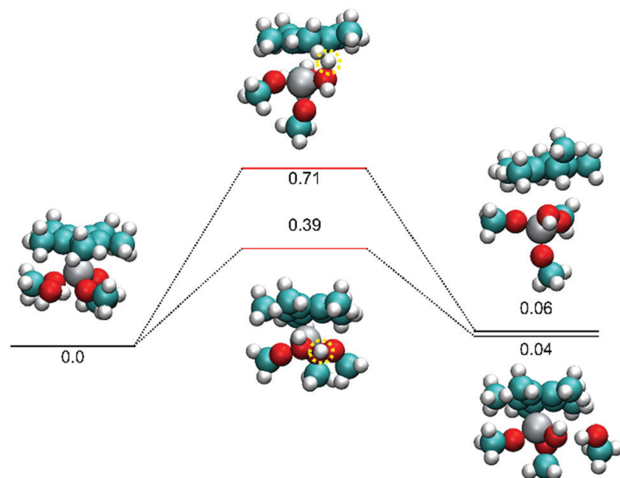

Fig. 1 Reaction between the Ti precursor and a water molecule. Black lines indicate reactant and product states, and the red lines indicate transition states. Yellow circles indicate transferred hydrogens. White, emerald, red, and gray spheres represent hydrogen, carbon, oxygen, and titanium atoms, respectively. Numbers are internal energies in the electron volt unit.

higher than that of the reactant state, the reaction can be driven by entropy. It is also important to note that although the B3LYP hybrid exchange–correlation functional is used in the calculations for accuracy, it underestimates the activation energies. Hence, the actual activation energies are likely larger.

The hydroxyl ligand significantly reduced the steric hindrance compared to the methoxy ligand. First-principles atomistic scale simulations were used to estimate the difference in the amount of chemisorbed precursor (Fig. 2). In the presence of methoxy ligands, one out of every three adsorption sites was blocked owing to the steric hindrance in the [−110] direction (Fig. 2(a)). Both the Cp* and methoxy ligands are sources of significant steric hindrance. Although the precursors can occupy two adsorption sites in a row in the [−110] direction, the steric hindrance tilts them in the opposite directions (Fig. 2(a) and (b)). Hence, the precursor cannot be adsorbed to the nearest adsorption sites next to the precursor pair. If the methoxy ligands are replaced with hydroxyl ligands, the steric hindrance is significantly decreased. The precursor with the hydroxyl ligands can occupy every adsorption site along the [−110] direction (Fig. 2(c)). In the [001] direction, the precursor occupies three adsorption sites regardless of whether it has methoxy ligands or hydroxyl ligands. As shown in Fig. 2(a) and (b), the chemisorbed precursor density is 1.15 nm^{-2}, while as shown in Fig. 2(c) it is 1.72 nm^{-2}. A simple change of ligands from methoxy to hydroxyl can enhance the chemisorbed precursor density by 50%.

The change in the GPC of TiO_2 ALD with respect to the sequence has been investigated to confirm the experimental implementation of the theoretically calculated increase in the GPC, through H_2O. In this study, the Ti precursor employed in the TiO_2 ALD reacts only with O_3. Even at a higher temperature of 390 °C, the Ti precursor does not react with H_2O (data not shown). This result might have originated from the reactivity difference between O_3 and H_2O. The GPC of TiO_2 ALD with O_3 was 0.034 nm per cycle. This GPC value is in agreement with the previous results of TiO_2 ALD with a heteroleptic Ti precursor.[35] This is because of the steric hindrance originating from the bulky geometry of the Cp* ligand. The GPC in ALD is affected by the amount of chemisorbed precursor during the precursor pulse step. Also, the steric hindrance by the geometry of the ligand, where the precursor adsorbs chemically on the surface, is one of the most considerable factors for determining the GPC. Additionally, the Cp-based Ti precursor induces a certain GPC value in the TiO_2 ALD. The geometry of the ligand in the precursor generally changes during chemisorption because chemisorption involves a chemical reaction. Hence, the surface termination chemistry strongly affects the nature of chemisorption of the precursor, resulting in significant changes in the deposition behaviour.[40] Both O_3 and H_2O are the most widely used oxygen sources in ALD, but they induce different surface termination. Therefore, modified TiO_2 ALD sequence by employing additional H_2O feeding and purge steps right after the O_3 feeding and purge steps (Fig. 3(a)) was used to investigate the change in the growth behaviour with respect to the altered surface termination chemistry. The GPC value change depending on the H_2O feeding and purge time (Fig. 3(b) and (c))

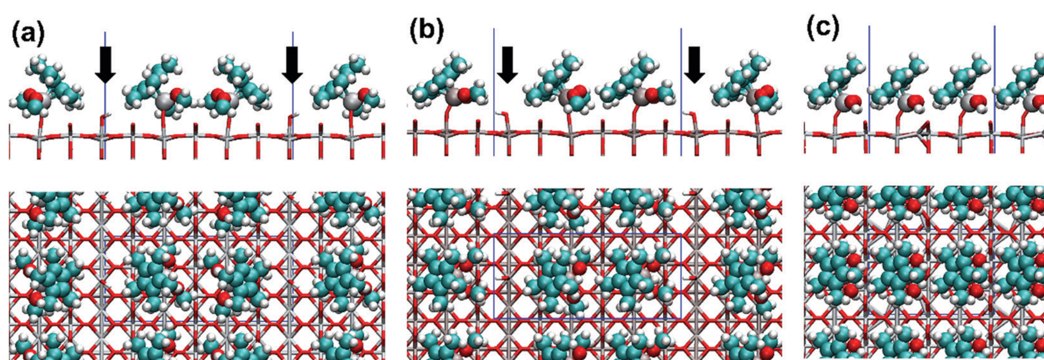

Fig. 2 Ti precursors covering the TiO_2(110) surface. In the presence of methoxy groups, the precursor cannot adsorb to one of every three rows of the adsorption sites due to the steric hindrance. (a and b) Those rows are denoted by black arrows. If methoxy groups are replaced with hydroxyl groups, the steric hindrance is alleviated and the precursor can adsorb to every row of the adsorption sites. (c) White, emerald, red, and gray spheres represent hydrogen, carbon, oxygen, and titanium atoms, respectively. Blue lines represent the periodic boundary used in calculations.

 This journal is © the Owner Societies 2021

Published on 01 October 2020. Downloaded by Kyunghee University on 3/24/2021 8:41:53 AM.

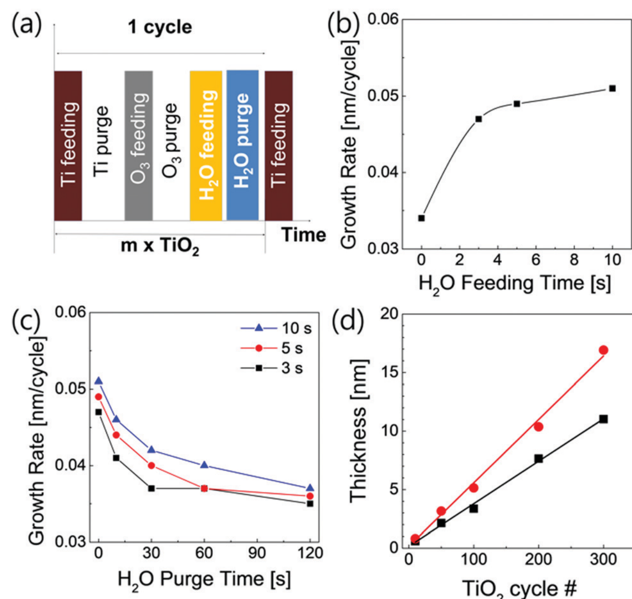

Fig. 3 (a) Schematic diagram of the H_2O-added sequence. (b) GPC change with respect to the H_2O feeding time. (c) GPC change with respect to the H_2O purge time at various H_2O feeding times of (black) 3, (red) 5, and (blue) 10 s. (d) Deposited TiO_2 thin film thickness with respect to the conducting TiO_2 ALD cycle number by (black) the conventional sequence, and (red) the H_2O-added sequence.

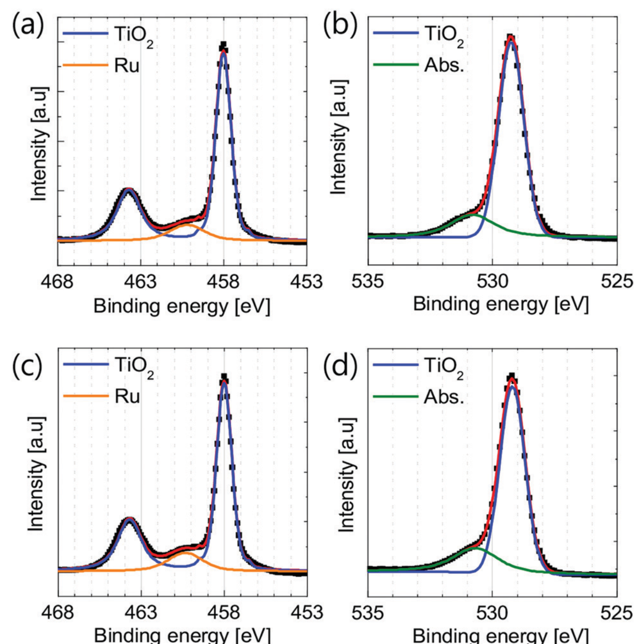

Fig. 4 Deconvoluted peaks of (a and c) the Ti 2p XPS and (b and d) O 1s XPS spectra, deposited by (a and b) the conventional sequence and (c and d) the H_2O-added sequence.

was evaluated. The additional H_2O step increased the GPC dramatically. The GPC of 0.034 nm per cycle in the conventional ALD sequence which consisted of the Ti precursor feeding and purge, also the O_3 feeding and purge steps, increased gradually with the increasing step time of the additionally introduced H_2O feeding time (10 s), and reached 0.052 nm per cycle, a value of approximately 1.53 times higher than the conventional sequence. Moreover, the GPC change by the additional H_2O step exhibited some characteristic behaviours with respect to the purge step time. The significant increase in GPC decreased when the H_2O purge time increased. In the case of an H_2O feeding time of 3 s, the GPC decreased to the same level as without the H_2O feeding where the purge time was increased up to 30 s. This H_2O purge time, where the GPC reached a conventional sequence level, was gradually increased to 60 and 120 s in the case of a H_2O feeding time of 5 and 10 s, respectively. The characteristic behaviour in the GPC caused by the additional H_2O step is summarized as follows: the additionally introduced H_2O contributes to increasing the GPC, the increasing GPC saturates with respect to the H_2O feeding time, and the GPC increasing effect disappeared with the increasing purge time. Furthermore, the increased GPC caused by the additional H_2O step was retained up to hundreds of ALD cycles (Fig. 3(d)), which indicates that the GPC enhancement is observed not only on the Ru substrate, but also on the fully covered surface deposited with the TiO_2 film.

These characteristic behaviours indicate that the introduced H_2O was adsorbed on the surface physically; this physisorbed H_2O contributed to the increase in GPC. Moreover, since the increase in GPC eventually saturated and H_2O did not react with the chemisorbed Ti precursor, the increase in p_{chem} of the Ti precursor can be attributed to H_2O changing the steric hindrance. These behaviours, especially the increment of GPC by ~50%, are consistent with the density functional theory (DFT) calculations.

Furthermore, the properties of the TiO_2 thin films deposited by the conventional and H_2O-added sequences were investigated to detect any degradation caused by the H_2O-added sequence. The chemical structures of the films were explored using XPS analysis. Fig. 4(a) and (c) shows the Ti 2p XPS spectra (data points) of the TiO_2 thin films deposited by the conventional without the H_2O sequence and with the H_2O-added sequence methods, respectively. Also, the deconvoluted spectra (lines) were obtained assuming that the Ti 2p peaks were composed of the Ti $2p_{3/2}$ peak centred at 458.0 and the Ru $3p_{3/2}$ peak centred at 460.2 eV, which correspond to TiO_2 and metallic Ru, respectively.[41] The XPS spectra of both the samples were almost identical regardless of the H_2O sequence. Moreover, the O 1s XPS spectra (Fig. 4(b) and (d)) also comprised the same oxygen components that were present in TiO_2 and absorbed on the surface.

The chemistry of the TiO_2 ALD also affects the crystallinity of the TiO_2 thin film deposited on the Ru substrate. In the case of the TiO_2 ALD on the Ru electrode, which utilizes O_3 as the oxygen source, the Ru substrate is oxidized by O_3 in an *in situ* manner;[41–43] the resulting ~1 nm thick RuO_2 induces phase transition of TiO_2 from anatase to rutile *via* the local epitaxial relationship. Consequently, any change in the chemistry during the TiO_2 ALD on the Ru substrate alters the crystallinity of the TiO_2 thin film. Fig. 5 shows the GIXRD pattern of the samples comprising a 20 nm thick TiO_2 thin film deposited on the Ru

Published on 01 October 2020. Downloaded by Kyunghee University on 3/24/2021 8:41:53 AM.

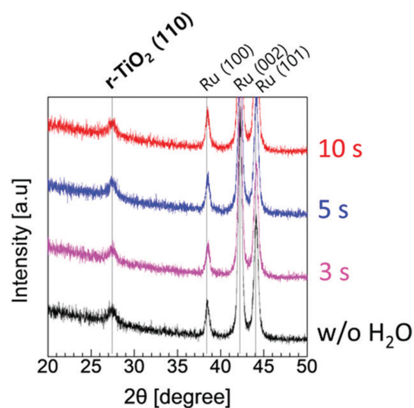

Fig. 5 XRD spectra of the TiO_2 thin film deposited by various sequences. Values in time (s) denote the H_2O feeding time in the H_2O-added sequence.

substrate under varying H_2O feeding time periods. All the as-deposited films were crystallized without any post-deposition annealing. The diffraction pattern of the TiO_2 thin film without the H_2O sequence indicated that the thin film comprised crystalline TiO_2 with a rutile structure. With the increasing H_2O feeding time, no significant change was observed in the diffraction peak of rutile TiO_2 at $2\theta = 27.3^{\circ}$, even for an H_2O feeding time of 10 s. The results obtained from the XPS and XRD analyses indicate that the physisorbed H_2O does not induce any change in the chemical reaction between the chemisorbed Ti precursor and O_3 by exhibiting no significant change in the chemical and physical structure of the TiO_2 thin film.

The electrical properties of the MIM capacitor employing a 20 nm thick TiO_2 thin film as an insulating layer also indicated the presence of identical physical and chemical structures, especially the crystallinity of the TiO_2 thin film deposited with the additional H_2O feeding step as compared to that of the film deposited *via* the conventional sequence. The bulk dielectric constant (k) was estimated from the inverse slope of the physical thickness (t_{phy}) *vs.* equivalent oxide thickness (t_{ox}) plot, where $t_{ox} = t_{phy}(3.9/k)$, because k represents the crystallinity of the TiO_2 thin film. As shown in Fig. 6(a), the k values of the TiO_2 thin films by conventional and H_2O-added sequences were 93.5 and 97.8, respectively. This result indicates that the TiO_2 thin films have identical crystallinity with the rutile phase. Moreover, the y-intercepts of the film by conventional and H_2O-added sequences were also identical to the values of 0.067 and 0.078 nm, respectively. The y-axis intercept in t_{ox} *vs.* t_{phy} plot is determined by the interfacial properties between the TiO_2 film and the TE or the BE, implying that the additional H_2O step does not induce any change at the interface of the TE or the BE. Hence, the leakage current density *vs.* applied voltage (J–V) curve of the MIM structure, which comprised the TiO_2 thin film deposited by the H_2O-added sequence, was identical to that of the film deposited *via* the conventional sequence (Fig. 6(b)). In the J–V curve of the MIM comprising TiO_2 deposited *via* the conventional sequence, the J value is significantly higher in the positive applied voltage region than in the negative region. This is due to the relatively defective interfacial properties between Ru BE and the TiO_2 thin film, which is caused by the damage to Ru BE due to O_3 during the deposition. The asymmetric J–V curve of the H_2O-added sequence also demonstrated identical characteristics. Fig. 6(c) shows the summary of the electrical performances of both (conventional and H_2O-added sequence) the films, which shows the variation of J estimated at +0.8 V as a function of t_{ox}. Since these two types of TiO_2 thin films have the exact same physical and chemical properties, all the points from the two TiO_2 thin films lie on the same trend in the J–t_{ox} curve.

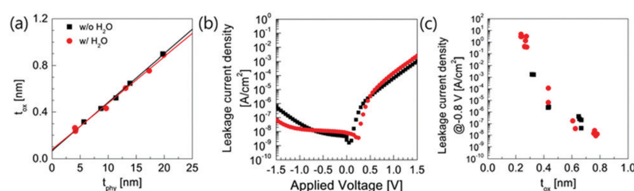

Fig. 6 (a) t_{phy}–t_{ox} plot, (b) J–V plot, and (c) J–t_{ox} plot of the MIM capacitor with 20 nm-thick TiO_2 deposited by (black) the conventional sequence and (red) the H_2O-added sequence with a H_2O feeding time of 10 s.

Conclusions

A theoretical and experimental approach to ALD has been proposed based on DFT to significantly improve the GPC of TiO_2 ALD, which is considered to be the most limiting characteristic of ALD. The calculation of the chemisorption reaction of $Ti(CpMe_5)(OMe)_3$ in the TiO_2 ALD, which has a low GPC due to its bulky ligand structure, revealed that the OCH_3 group also participates in inducing severe steric hindrance. The OCH_3 ligand can be changed to a smaller ligand of OH using H_2O. Eventually, p_{chem} increases by 50% due to the reaction of H_2O and OCH_3. The GPC of TiO_2 ALD increased by 53% when H_2O is introduced *via* an added sequence, which is consistent with the increase in GPC calculated by DFT. Moreover, the increase in GPC eventually saturated as indicated by the DFT calculation, thereby successfully completing the objective of the study.

Conflicts of interest

There are no conflicts to declare.

Acknowledgements

This work was supported by the Technology Innovation Program (No. 20003555) funded by the Ministry of Trade, Industry & Energy (MOTIE, Korea) and the National Research Foundation of Korea (NRF) grant funded by the Korea government (MSIT) (No. 2018R1C1B5045854, and 2019R1A6C1010052). The authors gratefully acknowledge SK Trichem Co., Ltd for supporting this work as a precursor supplier.

Published on 01 October 2020. Downloaded by Kyunghee University on 3/24/2021 8:41:53 AM.

References

1 J. S. Ponraj, G. Attolini and M. Bosi, *Crit. Rev. Solid State Mater. Sci.*, 2013, **38**, 203–233.
2 V. Cremers, R. L. Puurunen and J. Dendooven, Conformality in atomic layer deposition: current status overview of analysis and modelling, *Appl. Phys. Rev.*, 2019, **6**, 021302.
3 P. O. Oviroh, R. Akbarzadeh, D. Pan, R. A. M. Coetzee and T. C. Jen, New development of atomic layer deposition: processes, methods and applications, *Sci. Technol. Adv. Mater.*, 2019, **20**, 465–496.
4 R. W. Johnson, A. Hultqvist and S. F. Bent, *Mater. Today*, 2014, **17**, 236–246.
5 S. M. George, Atomic layer deposition: an overview, *Chem. Rev.*, 2010, **110**, 111–131.
6 M. Leskelä and M. Ritala, Atomic layer deposition chemistry: recent developments and future challenges, *Angew. Chem., Int. Ed.*, 2003, **42**, 5548–5554.
7 *Atomic Layer Deposition for Semiconductors*, ed. C.S. Hwang, Springer Science & Business Media, 2013.
8 C. Zhao and J. Xiang, Atomic layer deposition (ALD) of metal gates for CMOS, *Appl. Sci.*, 2019, **9**, 2388.
9 B. H. Lee, J. K. Hwang, J. W. Nam, S. U. Lee, J. T. Kim, S. M. Koo, A. Baunemann, R. A. Fischer and M. M. Sung, Low-temperature atomic layer deposition of copper metal thin films: self-limiting surface reaction of copper dimethylamino-2-propoxide with diethylzinc, *Angew. Chem., Int. Ed.*, 2009, **48**, 4536–4539.
10 W. Jeon, Recent advances in the understanding of high- k dielectric materials deposited by atomic layer deposition for dynamic random-access memory capacitor applications, *J. Mater. Res.*, 2019, 1–20.
11 J. P. Niemelä, G. Marin and M. Karppinen, Titanium dioxide thin films by atomic layer deposition: a review, *Semicond. Sci. Technol.*, 2017, **32**, 093005.
12 J. A. Kittl, K. Opsomer, M. Popovici, N. Menou, B. Kaczer, X. P. Wang, C. Adelmann, M. A. Pawlak, K. Tomida, A. Rothschild, B. Govoreanu, R. Degraeve, M. Schaekers, M. Zahid, A. Delabie, J. Meersschaut, W. Polspoel, S. Clima, G. Pourtois, W. Knaepen, C. Detavernier, V. V. Afanas'ev, T. Blomberg, D. Pierreux, J. Swerts, P. Fischer, J. W. Maes, D. Manger, W. Vandervorst, T. Conard, A. Franquet, P. Favia, H. Bender, B. Brijs, S. Van Elshocht, M. Jurczak, J. Van Houdt and D. J. Wouters, High-k dielectrics for future generation memory devices (invited paper), *Microelectron. Eng.*, 2009, **86**, 1789–1795.
13 J. Robertson, High dielectric constant gate oxides for metal oxide Si transistors, *Rep. Prog. Phys.*, 2006, **69**, 327–396.
14 S. K. Kim, K. M. Kim, D. S. Jeong, W. Jeon, K. J. Yoon and C. S. Hwang, Titanium dioxide thin films for next-generation memory devices, *J. Mater. Res.*, 2013, **28**, 313–325.
15 S. W. Lee, B. J. Choi, T. Eom, J. H. Han, S. K. Kim, S. J. Song, W. Lee and C. S. Hwang, Influences of metal, non-metal precursors, and substrates on atomic layer deposition processes for the growth of selected functional electronic materials, *Coord. Chem. Rev.*, 2013, **257**, 3154–3176.
16 A. Bin Afif, A. L. Dadlani, S. Burgmann, P. Köllensperger and J. Torgersen, Atomic layer deposition of perovskites—part 1: fundamentals of nucleation and growth, *Mater. Des. Process. Commun.*, 2020, **2**, 1–7.
17 A. J. M. Mackus, J. R. Schneider, C. MacIsaac, J. G. Baker and S. F. Bent, Synthesis of Doped, Ternary, and Quaternary Materials by Atomic Layer Deposition: A Review, *Chem. Mater.*, 2019, **31**, 1142–1183.
18 J. H. Shim, H. J. Choi, Y. Kim, J. Torgersen, J. An, M. H. Lee and F. B. Prinz, Process-property relationship in high-: K ALD SrTiO3 and BaTiO3: a review, *J. Mater. Chem. C*, 2017, **5**, 8000–8013.
19 J.-H. Ahn, S.-W. Kang, J.-Y. Kim, J.-H. Kim and J.-S. Roh, Effect of Sr–Ruthenate Seed Layer on Dielectric Properties of SrTiO[sub 3] Thin Films Prepared by Plasma-Enhanced Atomic Layer Deposition, *J. Electrochem. Soc.*, 2008, **155**, G185.
20 H. G. Kim and H.-B.-R. Lee, Atomic Layer Deposition on 2D Materials, *Chem. Mater.*, 2017, **29**, 3809–3826.
21 T. Nam, S. Seo and H. Kim, Atomic layer deposition of a uniform thin film on two-dimensional transition metal dichalcogenides, *J. Vac. Sci. Technol., A*, 2020, **38**, 030803.
22 M. Mattinen, T. Hatanpää, T. Sarnet, K. Mizohata, K. Meinander, P. J. King, L. Khriachtchev, J. Räisänen, M. Ritala and M. Leskelä, Atomic Layer Deposition of Crystalline MoS2 Thin Films: New Molybdenum Precursor for Low-Temperature Film Growth, *Adv. Mater. Interfaces*, 2017, **4**, 1–11.
23 J. J. Pyeon, S. H. Kim, D. S. Jeong, S.-H. Baek, C.-Y. Kang, J.-S. Kim and S. K. Kim, Wafer-scale growth of MoS 2 thin films by atomic layer deposition, *Nanoscale*, 2016, **8**, 10792–10798.
24 W. Jeon, Y. Cho, S. Jo, J.-H. Ahn and S.-J. Jeong, Wafer-Scale Synthesis of Reliable High-Mobility Molybdenum Disulfide Thin Films via Inhibitor-Utilizing Atomic Layer Deposition, *Adv. Mater.*, 2017, **29**, 1703031.
25 T. Jurca, M. J. Moody, A. Henning, J. D. Emery, B. Wang, J. M. Tan, T. L. Lohr, L. J. Lauhon and T. J. Marks, Low-Temperature Atomic Layer Deposition of MoS 2 Films, *Angew. Chem., Int. Ed.*, 2017, **56**, 4991–4995.
26 S.-J. Jeong, Y. Gu, J. Heo, J. Yang, C.-S. Lee, M.-H. Lee, Y. Lee, H. Kim, S. Park and S. Hwang, Thickness scaling of atomic-layer-deposited HfO2 films and their application to wafer-scale graphene tunnelling transistors, *Sci. Rep.*, 2016, **6**, 20907.
27 S.-J. Jeong, H. W. Kim, J. Heo, M.-H. Lee, H. J. Song, J. Ku, Y. Lee, Y. Cho, W. Jeon, H. Suh, S. Hwang and S. Park, Physisorbed-precursor-assisted atomic layer deposition of reliable ultrathin dielectric films on inert graphene surfaces for low-power electronics, *2D Mater.*, 2016, **3**, 035027.
28 Y. Lee, W. Jeon, Y. Cho, M.-H. Lee, S.-J. Jeong, J. Park and S. Park, Mesostructured Hf x Al y O 2 Thin Films as Reliable and Robust Gate Dielectrics with Tunable Dielectric Constants for High-Performance Graphene-Based Transistors, *ACS Nano*, 2016, **10**, 6659–6666.
29 Y. Li, Y. Xiong, H. Yang, K. Cao and R. Chen, Thin film encapsulation for the organic light-emitting diodes display via atomic layer deposition, *J. Mater. Res.*, 2020, **35**, 681–700.

Published on 01 October 2020. Downloaded by Kyunghee University on 3/24/2021 8:41:53 AM.

30 S. Lee, J. H. Han, S. H. Lee, G. H. Baek and J. S. Park, Review of Organic/Inorganic Thin Film Encapsulation by Atomic Layer Deposition for a Flexible OLED Display, *JOM*, 2019, **71**, 197–211.

31 N. Sobel and C. Hess, Nanoscale Structuring of Surfaces by Using Atomic Layer Deposition, *Angew. Chem., Int. Ed.*, 2015, **54**, 15014–15021.

32 A. J. M. Mackus, M. J. Weber, N. F. W. Thissen, D. Garcia-Alonso, R. H. J. Vervuurt, S. Assali, A. A. Bol, M. A. Verheijen and W. M. M. Kessels, Atomic layer deposition of Pd and Pt nanoparticles for catalysis: on the mechanisms of nanoparticle formation, *Nanotechnology*, 2016, **27**, 034001.

33 H. Van Bui, F. B. Wiggers, A. Gupta, M. D. Nguyen, A. A. I. Aarnink, M. P. de Jong and A. Y. Kovalgin, Initial growth, refractive index, and crystallinity of thermal and plasma-enhanced atomic layer deposition AlN films, *J. Vac. Sci. Technol., A*, 2015, **33**, 01A111.

34 A. Yanguas-Gil, K. E. Peterson and J. W. Elam, Controlled Dopant Distribution and Higher Doping Efficiencies by Surface-Functionalized Atomic Layer Deposition, *Chem. Mater.*, 2011, **23**, 4295–4297.

35 A. L. Johnson and J. D. Parish, *Recent developments in molecular precursors for atomic layer deposition*, 2018, vol. 1311.

36 M. J. Frisch, G. W. Trucks, H. B. Schlegel, G. E. Scuseria, M. A. Robb, J. R. Cheeseman, G. Scalmani, V. Barone, G. A. Petersson, H. Nakatsuji, X. Li, M. Caricato, A. V. Marenich, J. Bloino, B. G. Janesko, R. Gomperts, B. Mennucci, H. P. Hratchian, J. V. Ortiz, A. F. Izmaylov, J. L. Sonnenberg, D. Williams-Young, F. Ding, F. Lipparini, F. Egidi, J. Goings, B. Peng, A. Petrone, T. Henderson, D. Ranasinghe, V. G. Zakrzewski, J. Gao, N. Rega, G. Zheng, W. Liang, M. Hada, M. Ehara, K. Toyota, R. Fukuda, J. Hasegawa, M. Ishida, T. Nakajima, Y. Honda, O. Kitao, H. Nakai, T. Vreven, K. Throssell, J. A. Montgomery, Jr., J. E. Peralta, F. Ogliaro, M. J. Bearpark, J. J. Heyd, E. N. Brothers, K. N. Kudin, V. N. Staroverov, T. A. Keith, R. Kobayashi, J. Normand, K. Raghavachari, A. P. Rendell, J. C. Burant, S. S. Iyengar, J. Tomasi, M. Cossi, J. M. Millam, M. Klene, C. Adamo, R. Cammi, J. W. Ochterski, R. L. Martin, K. Morokuma, O. Farkas, J. B. Foresman and D. J. Fox, *Gaussian 16, Revision A.03*, Gaussian, Inc., Wallingford CT, 2016.

37 S. Grimme, J. Antony, S. Ehrlich and H. Krieg, A consistent and accurate ab initio parametrization of density functional dispersion correction (DFT-D) for the 94 elements H-Pu, *J. Chem. Phys.*, 2010, **132**, 154104.

38 G. Kresse and J. Furthmüller, Efficient iterative schemes for *ab initio* total-energy calculations using a plane-wave basis set, *Phys. Rev. B: Condens. Matter Mater. Phys.*, 1996, **54**, 11169–11186.

39 A. Zydor and S. D. Elliott, TiCp*$(OMe)_3$ versus $Ti(OMe)_4$ in atomic layer deposition of TiO_2 with water – Ab initio modelling of atomic layer deposition surface reactions, *J. Nanosci. Nanotechnol.*, 2011, **11**, 8089–8093.

40 M. J. Chung, W. Jeon, C. H. An, S. H. Kim, Y. K. Lee, W. Lee and C. S. Hwang, Quantitative Analysis of the Incorporation Behaviors of Sr and Ti Atoms During the Atomic Layer Deposition of $SrTiO_3$ Thin Films, *ACS Appl. Mater. Interfaces*, 2018, **10**, 8836–8844.

41 W. Jeon, W. Lee, Y. W. Yoo, C. H. An, J. H. Han, S. K. Kim and C. S. Hwang, Chemistry of active oxygen in RuO_x and its influence on the atomic layer deposition of TiO_2 films, *J. Mater. Chem. C*, 2014, **2**, 9993–10001.

42 S. K. Kim, G.-J. Choi, S. Y. Lee, M. Seo, S. W. Lee, J. H. Han, H.-S. Ahn, S. Han and C. S. Hwang, Al-Doped TiO_2 Films with Ultralow Leakage Currents for Next Generation DRAM Capacitors, *Adv. Mater.*, 2008, **20**, 1429–1435.

43 S. K. Kim, W. D. Kim, K. M. Kim, C. S. Hwang and J. Jeong, High dielectric constant TiO_2 thin films on a Ru electrode grown at 250 °C by atomic-layer deposition, *Appl. Phys. Lett.*, 2004, **85**, 4112–4114.

This journal is © the Owner Societies 2021